



Real-time electrical detection of the formation and destruction of lipid bilayers on silicon nanowire devices



Elissa H. Williams^{a,b,c,*}, Jong-Yoon Ha^{c,d}, Melanie Juba^a, Barney Bishop^a, Sergiy Krylyuk^{c,d}, Abhishek Motayed^{c,d}, Mulpuri V. Rao^b, John A. Schreifels^a, Albert V. Davydov^c

^a Department of Chemistry and Biochemistry, George Mason University, 4400 University Drive, Fairfax, VA 22030, USA

^b Department of Electrical and Computer Engineering, George Mason University, 4400 University Drive, Fairfax, VA 22030, USA

^c Material Measurement Laboratory, National Institute of Standards and Technology, 100 Bureau Drive, Gaithersburg, MD 20899, USA

^d Institute for Research in Electronics and Applied Physics, University of Maryland, College Park, MD 20742, USA

ARTICLE INFO

Keywords:

Nanowire biosensor
Two-terminal device
Lipid bilayer
Cell membrane
Escherichia coli

ABSTRACT

Silicon nanowire (Si NW) two-terminal devices were fabricated to electrically probe the real-time formation and destruction of lipid bilayers. A liposome solution, containing the same ratio of zwitterionic/anionic lipids that are present in an *Escherichia coli* cell membrane, was applied to the NW devices. Lipid bilayer formation on the Si NWs was detected in-situ by observing electrical resistance changes complemented by confocal fluorescence microscopy imaging. The formation of lipid bilayers resulted in a 1% to 2% decrease in device current, consistent with the negative gating effect of the lipids on the NW surface. The devices demonstrated a ≈ 1 min electrical response time to lipid encapsulation. Removal of the lipid layer was achieved by exposing the devices to a detergent, which resulted in NW conductance returning to its original value with a ≈ 2 min recovery time. The lipid bilayer coated Si NWs demonstrate a novel platform to enable in-situ electrical probing of bacterial cell membrane mechanisms, interactions, and reactions.

© 2015 The Authors. Published by Elsevier B.V. This is an open access article under the CC BY-NC-ND license (<http://creativecommons.org/licenses/by-nc-nd/4.0/>).

1. Introduction

Over the past decade, silicon (Si) nanowires (NWs) have been studied extensively as biosensing platforms. Due to the fact that biomolecules can act as an electrical gate upon adsorption onto NW surfaces and change NW device conductivity, the label-free, real-time electrical detection of a wide variety of biomolecules has been realized [1–7]. The high surface-to-volume ratio of the electrically active NW enables its extremely high sensitivity to analytes, while selectivity is realized through biomolecule specific NW surface functionalization.

The success of Si NW devices in the detection of biological compounds has opened up the possibility of using NWs to study the mechanisms of cellular reactions [8,9]. Since cell membranes play

a critical role in cellular interactions, studies have recently been carried out to encapsulate NWs in a lipid bilayer as to mimic a cell membrane [9–12]. The electrical detection of ion transport through pore channels in a lipid bilayer coated Si NW was recently demonstrated in [13], revealing the potential of using Si NW devices as artificial cell constructs.

While the in-situ formation of lipid bilayers on Si NWs was studied using fluorescence microscopy in [12], real-time electrical measurements performed to analyze the temporal effect of the membrane formation process on NW conductivity were absent. A change in the electrical resistance for a bilayer coated vs. uncoated NW was demonstrated only ex-situ by Misra et al. [13] and Martinez et al. [10]. In this paper, we sought out to study in-situ lipid bilayer formation and destruction on Si NW surfaces using electrical measurements, complimented by ex-situ confocal fluorescence microscopy imaging. Liposomes consisting of 80% zwitterionic lipids (phosphatidylcholine (PC)) and 20% anionic lipids (phosphatidylglycerol (PG)) were utilized to mimic the charged lipids present in an *Escherichia coli* cell membrane [14]. The liposomes were applied to Si NW devices to study lipid bilayer formation and a common detergent, Tween20, was used to remove the lipid layer from the NW surface [15]. This work demonstrates that

* Corresponding author at: Department of Chemistry and Biochemistry, George Mason University, 4400 University Drive, Fairfax, VA 22030, USA. Tel.: +1 703 993 1070; fax: +1 703 993 1055.

E-mail addresses: ewilliah@gmu.edu (E.H. Williams), jongyoon.ha@nist.gov (J.-Y. Ha), mjuba@gmu.edu (M. Juba), bbishop1@gmu.edu (B. Bishop), sergiy.krylyuk@nist.gov (S. Krylyuk), abhishek.motayed@nist.gov (A. Motayed), rmulpuri@gmu.edu (M.V. Rao), jschreif@gmu.edu (J.A. Schreifels), albert.davydov@nist.gov (A.V. Davydov).

changes in NW electrical conductivity directly correlate to the formation and the consecutive removal of lipid bilayers over NW surfaces. The membrane encapsulated two-terminal Si NW devices demonstrated here present a novel platform to enable the electrical probing of bacterial cell membrane reactions.

2. Materials and methods

2.1. Device design

A schematic of the Si NW sensor chip utilized in the experiments is shown in Fig. 1(A). The 25 mm × 25 mm chip included twelve 1 mm × 1 mm electrical contact pads at the top of the sensor chip (see Section 2.5 below for more details). The twelve metal pads extended as 20 μm wide lines to the center of the chip where they paired at a 10 μm gap. As shown in Fig. 1(B), a single Si NW bridged each gap resulting in a total of six NW devices on the chip. A 5 μm wide, 6 mm long photolithographically etched channel encompassed all six NW devices and connected to a fluid reservoir at the bottom of the chip (see Fig. 1(A) and (B)).

2.2. Device fabrication

A 4" Si (100) wafer, coated with a 300 nm SiO₂ layer (see Fig. 2, A1), was utilized as the substrate for device fabrication. The wafer was diced into 25 mm × 25 mm squares, cleaned using acetone and isopropanol, rinsed in distilled water, and then dried using a stream of nitrogen. Photolithography processing steps defined the openings for the bottom metal contacts (Fig. 2, A2) followed by electron beam deposition of 15 nm of Ti metal (Fig. 2, A3). N-type Si NWs, with a length of about 30 μm and a diameter of 120 nm, grown using catalyst assisted vapor–liquid–solid chemical vapor deposition [16], were dielectrophoretically aligned onto the Ti contact pads (Fig. 2, A4) as described in our previous paper [17]. Dielectrophoretic alignment was carried out at 20 V to 30 V of alternating current at 1 kHz. Photolithography steps were utilized to define openings for the top metal contacts (Fig. 2, A5). Electron beam deposition was used to deposit a stack of metals (70 nm of Ti, 70 nm of Al, 50 nm of Ti, and 50 nm of Au) onto the patterned chips (Fig. 2, A6). The completed devices were annealed in argon at 550 °C for 30 s to facilitate ohmic contact formation (Fig. 2, A7).

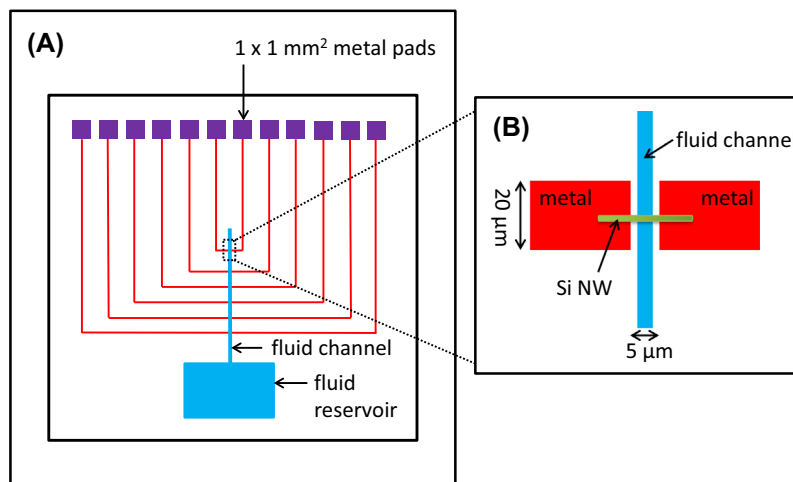


Fig. 1. (A) The design schematic of the Si NW sensor chip. The chip contained six two-terminal NW devices, a fluid channel, and a fluid reservoir. (B) An enlarged region of one of the six NW devices.

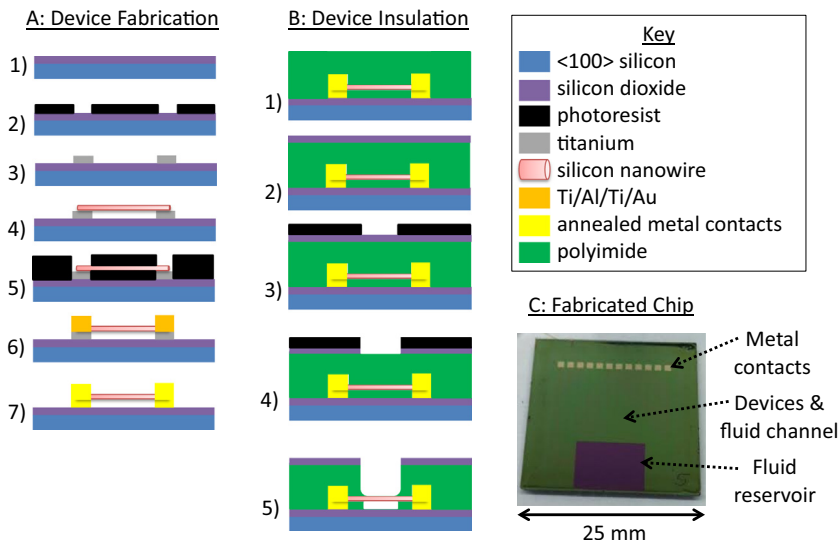


Fig. 2. Si NW sensor chip fabrication (A) and insulation (B) steps. An optical image of a fabricated and insulated sensor chip is shown in (C).

2.3. Device insulation

To insulate the Si NW devices for the application of ionically conducting fluids, approximately 3 μm thick polyimide (PI) was spun onto the surface of the sensor chip (Fig. 2, B1). Following a baking and curing of the polyimide, 100 nm of SiO_2 was deposited onto the chips using plasma enhanced chemical vapor deposition (Fig. 2, B2). Standard photolithography steps were utilized to define a 5 μm wide channel to guide the flow of liquids over the center of the Si NWs (see Fig. 2, B3). A CHF_3/O_2 plasma etch was used to etch through the deposited oxide layer (see Fig. 2, B4). Then, an O_2 plasma was used to etch through the polyimide and to remove the top photoresist layer (Fig. 2, B5) An optical image of a fabricated and insulated sensor chip is shown in Fig. 2(C).

2.4. Preparation of liposomes and Tween20 solution

Small unilamellar vesicles (SUVs) were prepared using DOPC (1,2-dioleoyl-sn-glycero-3-phosphocholine, 5 mg/mL in chloroform, Avanti Polar Lipids), DOPG (1,2-dioleoyl-sn-glycero-3-[phospho-o-rac-(1-glycerol)] (sodium salt), 1 mg/mL in chloroform, Avanti Polar Lipids), and NBD-PG (1-oleoyl-2-{6-[(7-nitro-2-1,3-benzoxadiazol-4-yl)amino]hexanoyl}-sn-glycerol-3-[phospho-rac-(1-glycerol)] (ammonium salt), 1 mg/mL in chloroform, Avanti Polar Lipids).¹ 80% DOPC, 18% DOPG, and 2% NBD-PG (mole percent) were added to a round bottom flask using gas tight syringes. The solution was rotor-evaporated with a nitrogen gas flow followed by vacuum drying to evaporate chloroform. The lipids were resuspended in phosphate buffer, 0.01 M, pH = 7.4, to produce a final lipid concentration of 2.5 mg/mL. The lipid solution was rotor-evaporated without gas flow to ensure complete resuspension of the lipids in buffer. The lipid solution was extruded through an Avanti Mini Extruder, using a 50 nm polycarbonate filter, for 10 total pass throughs to give 50 nm liposomes suspended in buffer [18]. Following 24 h from liposome preparation, liposome solutions were sonicated for 30 min to ensure SUVs.

The common biological detergent, Tween20 (polyethylene glycol sorbitan monolaurate, viscous liquid, Sigma–Aldrich), was dissolved in phosphate buffer (0.01 M, pH = 7.4) to make a 10% by volume solution.

2.5. Device testing

The 1 mm \times 1 mm metal pads (at the top of the sensor chip) were connected to an Agilent Semiconductor Parameter Analyzer system. For the current–voltage (I–V) measurements, the devices were subjected to a 5 V to –5 V voltage sweep. For current versus time measurements, a constant voltage of 500 mV was applied to the devices and current values were recorded every second. 10 μL to 100 μL drops of phosphate buffer (0.01 M, pH = 7.4), liposome solution, and 10% Tween20 solution were applied to the fluid channel of the Si NW sensor chip using a pipette and the current of the NW as a function of time was recorded.

2.6. Optical and fluorescence microscopy

Optical microscopy was performed on the Si NW sensor chips using an upright Olympus Optical Microscope. Images of the NW devices were obtained using a 50 \times or 100 \times objective in bright or dark field mode. Fluorescence microscopy was performed on the Si NW sensor chips using a Leica Microsystems Confocal Microscope equipped with a 40 \times water immersion objective. The

images were obtained for an emission wavelength range of 500 nm to 600 nm using a 458 nm excitation wavelength.

3. Results and discussion

3.1. Characterization of the Si NW devices

The I–V characteristics of a Si NW device on a fabricated and insulated sensor chip are shown in Fig. 3(A). Before the annealing step, the devices displayed a non-linear I–V dependence due to the non-ohmic behavior of the electrical contacts. After annealing, the devices demonstrated a linear I–V relationship with much higher current values due to ohmic contact formation. Following the deposition of the polyimide insulation layer on the sensor chip, the Si NW devices retained linear I–V behavior with slightly decreased current values. Optical microscopy images of a Si NW device before and after annealing, and after polyimide insulation are shown in Fig. 3(B)–(D).

3.2. Sensor chip device testing

The Si NW sensor chip was connected to the Agilent Semiconductor Parameter Analyzer system as described in Section 2.5 for the biosensing experiments. The response of a Si NW device to phosphate buffer, PC/PG liposomes, and Tween20 is shown in Fig. 4. Before the start of the sensing experiment, the Si NW sensor chip was incubated in phosphate buffer. After a \approx 10 min incubation time, the sensing experiment began ($t = 0$) with an applied voltage of 500 mV. The device in the buffer solution demonstrated a current value of about 2.53 μA . To ensure that the Si NW device had reached a steady-state conductance, 20 μL of phosphate buffer was added three times to the sensor chip (see Fig. 4, circles marked as 1, 2, and 3 at \approx 50 s, \approx 200 s, and \approx 350 s, respectively). As a result, the current slightly decreased and reached a baseline value of 2.52 μA . A 60 μL drop of the PC/PG liposome solution (i.e. a bacterial cell membrane) was then added to the sensor chip (Fig. 4, see circle 4 at \approx 450 s). The current in the device decreased to 2.49 μA (a 1.2% decrease) and remained steady over the course of \approx 15 min. The decrease in NW current can be attributed to the formation of a lipid bilayer around the NW (described in more detail in Section 3.3). The response time of the device (defined as the time required for the device current to reach 80% of its total decrease in current) was 88 s. After a \approx 15 min exposure to the liposome solution, 30 μL of the Tween20 solution was added to the device (see Fig. 4, circle 5 at \approx 1350 s). The current in the NW increased to 2.525 μA (a 1.4% increase), which was the approximate baseline current value of the NW in phosphate buffer. The current increase corresponds to removing the lipid bilayer from the NW surface leading in a return of NW conductance to its original value (see a fluorescent microscopy verification experiment below and the mechanism Section 3.3 for more details). It is important to note that the recovery time for the device (defined as the time required for the device current to reach 80% of its total increase in current) was 124 s. Numerous Si NW devices were tested as described above. On average, the liposome solution resulted in a 1% to 2% decrease in NW conductance with a 1 min device response time. For all tested lipid encapsulated Si NW devices, the Tween20 solution resulted in the recovery of NW conductance to its baseline value in buffer with an average 2 min response time.

To confirm that the decrease in NW current (Fig. 4, circle marked as 4) was due to the formation of a lipid bilayer on the NW surface, confocal fluorescence microscopy was performed. The liposomes utilized in the experiments contained a green fluorophore and would result in green NW fluorescence if lipids did

¹ Commercial equipment and material suppliers are identified in this paper in order to adequately describe experimental procedures, which does not imply endorsement by NIST.

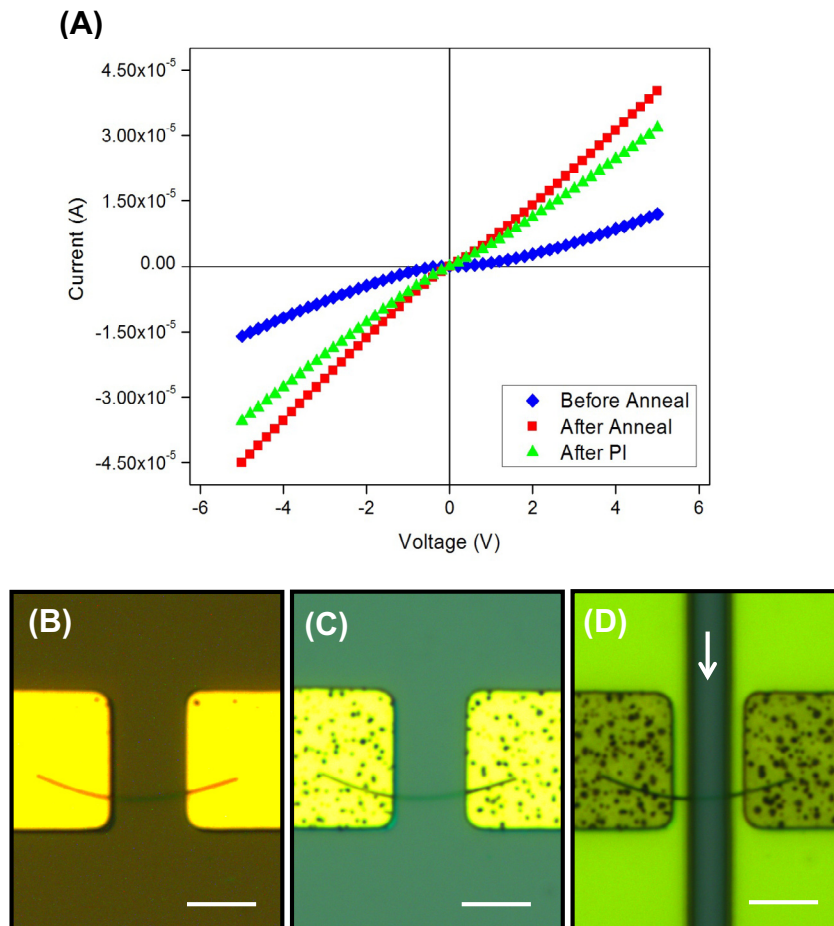


Fig. 3. (A) I–V curves for a Si NW device before anneal (blue diamonds), after anneal (red squares), and after polyimide (PI) insulation (green triangles). (B)–(D) Optical microscopy images of a Si NW device: (B) before anneal, (C) after anneal, and (D) after polyimide insulation. The arrow in (D) indicates the sensor chip fluid channel. Note that dark spots formed upon annealing due to reaction of metals in the pads. The scale bar in all three images is 10 μm . (For interpretation of the references to color in this figure legend, the reader is referred to the web version of this article.)

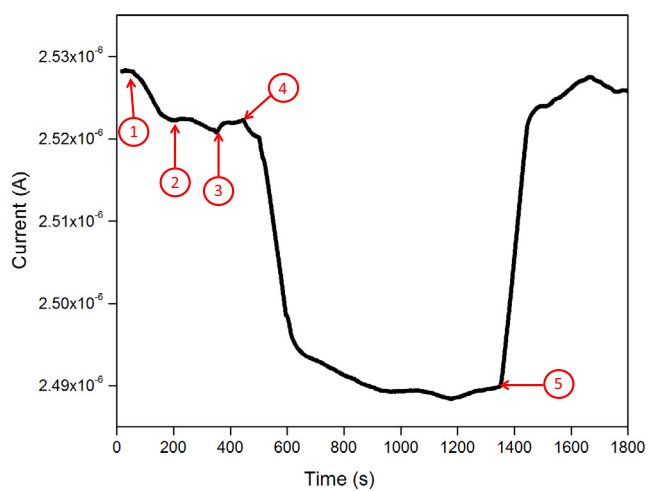


Fig. 4. Current versus time response of a Si NW device upon the addition of a 20 μL drop of phosphate buffer (1), (2), (3), 60 μL of PC/PG liposome solution (4), and 30 μL of Tween20 solution (5).

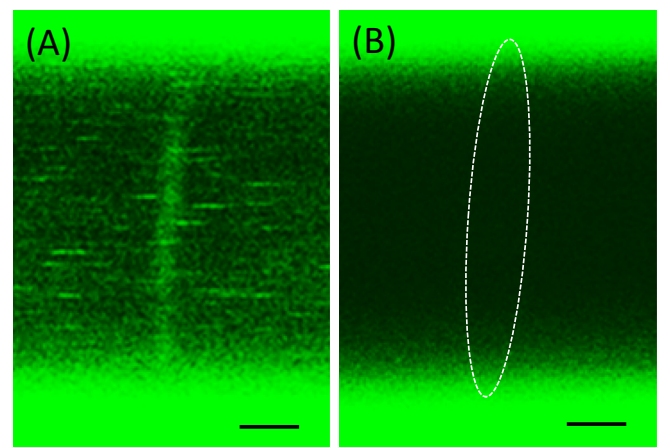


Fig. 5. (A) Confocal fluorescence microscopy of a Si NW after exposure to the PC/PG liposome solution. The fluorescing horizontal streaks are excess liposomes floating in solution. (B) The corresponding fluorescence image after exposure to the Tween20 solution. The dashed white line encircles the location of the non-fluorescing NW. Note that the polyimide insulation layer used in the experiments is inherently fluorescent and appears as the bright, fluorescent horizontal edges in both images. The scale bar in both images is 1 μm .

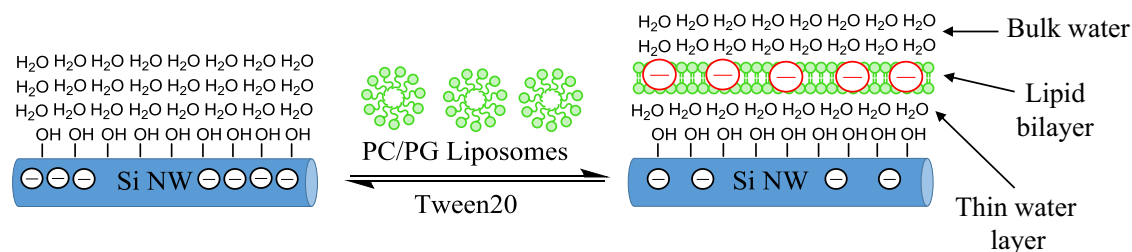


Fig. 6. Mechanism of lipid bilayer formation/destruction on a Si NW and its effect on NW conductance. The red/black circles with lines in their interior represent electrons. Note the schematic reduction of negative charges in the NW due to the gating effect of a lipid bilayer, which results in reduced NW conductivity. (For interpretation of the references to color in this figure legend, the reader is referred to the web version of this article.)

encapsulate the NW. Fig. 5(A) shows that the NW is fluorescing green following its exposure to the liposome solution (the image corresponds to the region between the circles marked 4 and 5 in Fig. 4). As a consequence, it can be concluded that the liposomes did encapsulate the NW leading to a decrease in device current. The average fluorescence intensity of the NW in Fig. 5(A) was 53 ± 13 . Because the NW fluorescence is relatively uniform, it is likely that a lipid bilayer, rather than lipid multilayers, formed on the NW surface [11]. Also, since the liposomes utilized in the experiments contained the same ratio of zwitterionic/anionic lipids as an *Escherichia coli* cell membrane, the lipid coating on the NWs mimics an *Escherichia coli* cell membrane at this stage in the experiments.

To confirm that the increase in NW conductance back to its original value in buffer (Fig. 4, circle marked as 5) was due to Tween20 removing the lipid bilayer from the NW surface, fluorescence microscopy was performed. Fig. 5(B) demonstrates a loss in the NW's fluorescence after Tween20 is applied to the sensor chip (this image corresponds to region 5, the end of the experiment, in Fig. 4). The average fluorescence intensity of the NW in Fig. 5(B) was 12 ± 1 . The lack of NW fluorescence indicates that the increase in NW conductance to its original baseline value was due to Tween20 destroying the lipid layer on the NW.

3.3. Mechanism of the formation and destruction of a lipid layer on NWs

Studies have been conducted to probe the formation of lipid bilayers on solid, planar substrates and it has been determined that liposome vesicles spontaneously break open and assemble into fluid bilayers on both silicon and quartz [19–21]. It is proposed that as vesicles form a bilayer on solid surfaces, a thin water layer acts as a cushion between the substrate and the supported bilayer, subsequently pushing the bulk of the water to the other side of the bilayer [19–21]. It is presumed that upon exposure of the NWs to the PC/PG liposomes in our experiments (Fig. 4, the circle marked as 4 and Fig. 5(A)), this type of mechanism also occurs (see Fig. 6). In addition, Noy's group proposed that formation of a water supported bilayer on NWs with diameters down to 20 nm is energetically favorable if the liposome vesicle diameter is less than 60 nm [11]. Due to the fact that in our experiments, 50 nm liposome vesicles and 120 nm wide NWs were utilized, spontaneous formation of a lipid membrane on NWs was favorable and was consistent with the electrical measurements and fluorescence microscopy imaging.

The PC/PG liposome solution and the resulting bilayer that is formed on the NW contains an overall net negative charge [18]. It is therefore expected that bilayer formation on the n-type Si NW surface would lead to a decrease in NW conductance due to gating effects; the charged lipid bilayer would result in a suppression of negative carriers at the NW surface, thus causing a surface

carrier depletion and a decrease in NW conductance [2,5]. The formation of a PC/PG bilayer on the Si NW devices did indeed lead to a reduction in NW conductance of about 1–2% in our experiments.

Tween20 is a commonly used detergent for lipid solubilization [15,22]. It is expected that upon exposure of a lipid encapsulated NW to a concentrated solution of Tween20, the lipid bilayer would be removed from the NW surface. In our experiments, the application of a 10% Tween20 solution to a lipid encapsulated NW (Fig. 4, the circle marked as 5) resulted in a return of the NW conductance to its original value in phosphate buffer. Therefore, we conclude that this increase in conductance is due to the removal of the lipid bilayer from the NW. The fluorescence microscopy results (Fig. 5(B)) confirm that no lipids remain immobilized on the Si NW surface after exposure to the Tween20 solution.

4. Conclusions

The design, fabrication, and insulation of a Si NW sensor chip to electrically probe the formation and destruction of a lipid bilayer was presented. Si NW devices were exposed to a PC/PG liposome solution, with the same ratio of zwitterionic/anionic lipids that are present in an *Escherichia coli* cell membrane. Lipid bilayer formation was found to occur on the Si NWs as was demonstrated by both electrical measurements and confocal fluorescence microscopy. The electrical measurements revealed a 1–2% decrease in NW conductance, with a 1 min response time upon lipid encapsulation. This decrease in NW conductance was attributed to the gating effect of the lipid bilayer on the surface of the n-type NW devices. The fluorescence microscopy images demonstrated relatively uniform NW fluorescence post exposure to the PC/PG liposome solution, likely indicating bilayer formation on the NW surface. The lipid encapsulated NW devices were exposed to a concentrated solution of detergent, Tween20. The Tween20 solution destroyed the lipid bilayer on the NW devices as was evidenced by both electrical and fluorescence microscopy measurements. The conductance in the NW returned to its original value in phosphate buffer within about a 2 min exposure period to the Tween20 solution, indicating the full removal of the lipid layer from the NW's surface. The corresponding fluorescence microscopy images confirmed removal of the lipids from the NWs. The studies presented demonstrate that the formation and destruction of a lipid layer mimicking an *Escherichia coli* cell membrane can be detected in-situ by electrical measurements and confocal fluorescence microscopy. The lipid encapsulated Si NW devices demonstrate a novel platform to further probe cell membrane biochemical processes.

Conflict of interest

The authors of this manuscript certify that this published work has no conflict of interests.

Acknowledgments

The authors are appreciative of the helpful discussions with Stoyan Jeliakov, Hany Issa, and Madhuri Mairipelly. EHW, MVR, and JAS gratefully acknowledge the financial support of the National Science Foundation (Grant # ECCS-0901712). The Si NW sensor chips were fabricated in the Nanofab facility of the NIST Center for Nanoscale Science and Technology.

References

- [1] G.-J. Zhang, Y. Ning, Silicon nanowire biosensor and its applications in disease diagnostics: a review, *Anal. Chim. Acta.* 749 (2012) 1–15, <http://dx.doi.org/10.1016/j.aca.2012.08.035>.
- [2] C.M. Lieber, F. Patolsky, Nanowire nanosensors, *Mater. Today* 8 (2005) 20–28.
- [3] Y. Cui, Q. Wei, H. Park, C.M. Lieber, Nanowire nanosensors for highly sensitive and selective detection of biological and chemical species, *Science* 293 (2001) 1289–1292, <http://dx.doi.org/10.1126/science.1062711>.
- [4] F. Patolsky, G. Zheng, C.M. Lieber, Fabrication of silicon nanowire devices for ultrasensitive, label-free, real-time detection of biological and chemical species, *Nat. Protoc.* 1 (2006) 1711–1724, <http://dx.doi.org/10.1038/nprot.2006.227>.
- [5] F. Patolsky, G. Zheng, C.M. Lieber, Nanowire-based biosensors, *Anal. Chem.* 78 (2006) 4260–4269.
- [6] Z. Gao, A. Agarwal, A.D. Trigg, N. Singh, C. Fang, C.-H. Tung, et al., Silicon nanowire arrays for label-free detection of DNA, *Anal. Chem.* 79 (2007) 3291–3297, <http://dx.doi.org/10.1021/ac061808q>.
- [7] G. Zheng, F. Patolsky, Y. Cui, W.U. Wang, C.M. Lieber, Multiplexed electrical detection of cancer markers with nanowire sensor arrays, *Nat. Biotech.* 23 (2005) 1294–1301, <http://dx.doi.org/10.1038/nbt1138>.
- [8] K.-I. Chen, B.-R. Li, Y.-T. Chen, Silicon nanowire field-effect transistor-based biosensors for biomedical diagnosis and cellular recording investigation, *Nano Today* 6 (2011) 131–154, <http://dx.doi.org/10.1016/j.nantod.2011.02.001>.
- [9] A. Noy, Bionanoelectronics, *Adv. Mater.* 23 (2011) 807–820, <http://dx.doi.org/10.1002/adma.201003751>.
- [10] J.A. Martinez, N. Misra, Y. Wang, P. Stroeve, C.P. Grigoropoulos, A. Noy, Highly efficient biocompatible single silicon nanowire electrodes with functional biological pore channels, *Nano Lett.* 9 (2009) 1121–1126, <http://dx.doi.org/10.1021/nl8036504>.
- [11] S.-C.J. Huang, A.B. Artyukhin, J.A. Martinez, D.J. Sirbully, Y. Wang, J.-W. Ju, et al., Formation, stability, and mobility of one-dimensional lipid bilayers on polysilicon nanowires, *Nano Lett.* 7 (2007) 3355–3359, <http://dx.doi.org/10.1021/nl071641w>.
- [12] L. Römhildt, A. Gang, L. Baraban, J. Opitz, G. Cuniberti, High yield formation of lipid bilayer shells around silicon nanowires in aqueous solution, *Nanotechnology* 24 (2013) 355601, <http://dx.doi.org/10.1088/0957-4484/24/35/355601>.
- [13] N. Misra, J.A. Martinez, S.-C.J. Huang, Y. Wang, P. Stroeve, C.P. Grigoropoulos, et al., Bioelectronic silicon nanowire devices using functional membrane proteins, *Proc. Natl. Acad. Sci.* 106 (2009) 13780–13784, <http://dx.doi.org/10.1073/pnas.0904850106>.
- [14] R.M. Epand, S. Rotem, A. Mor, B. Berno, R.F. Epand, Bacterial membranes as predictors of antimicrobial potency, *J. Am. Chem. Soc.* 130 (2008) 14346–14352, <http://dx.doi.org/10.1021/ja8062327>.
- [15] G.D. Noudeh, K. Payam, P. Rahmani, Study of the effects of polyethylene glycol sorbitan esters surfactants group on biological membranes, *Int. J. Pharmacol.* 4 (2008) 27–33. <<http://www.scialert.net/qredirect.php?doi=ijp.2008.27.33&linkid=pdf>>.
- [16] S. Krylyuk, A.V. Davydov, I. Levin, Tapering control of Si nanowires grown from SiCl₄ at reduced pressure, *ACS Nano* 5 (2011) 656–664, <http://dx.doi.org/10.1021/nn102556s>.
- [17] G.S. Aluri, A. Motayed, A.V. Davydov, V.P. Oleshko, K.A. Bertness, N.A. Sanford, et al., Methanol, ethanol and hydrogen sensing using metal oxide and metal (TiO₂)–Pt composite nanoclusters on GaN nanowires: a new route towards tailoring the selectivity of nanowire/nanocluster chemical sensors, *Nanotechnology* 23 (2012) 175501, <http://dx.doi.org/10.1088/0957-4484/23/17/175501>.
- [18] M. Juba, D. Porter, S. Dean, S. Gillmor, B. Bishop, Characterization and performance of short cationic antimicrobial peptide isomers, *Biopolymers* 100 (2013) 387–401, <http://dx.doi.org/10.1002/bip.22244>.
- [19] B.W. Koenig, S. Krueger, W.J. Orts, C.F. Majkrzak, N.F. Berk, J.V. Silverton, et al., Neutron reflectivity and atomic force microscopy studies of a lipid bilayer in water adsorbed to the surface of a silicon single crystal, *Langmuir* (1996) 1343–1350.
- [20] S.J. Johnson, T.M. Bayerl, D.C. McDermott, G.W. Adam, A.R. Rennie, R.K. Thomas, et al., Structure of an adsorbed dimyristoylphosphatidylcholine bilayer measured with specular reflection of neutrons, *Biophys. J.* 59 (1991) 289–294.
- [21] P.S. Cremer, S.G. Boxer, Formation and spreading of lipid bilayers on planar glass supports, *J. Phys. Chem B* 291 (1999) 2554–2559.
- [22] M. le Maire, P. Champeil, J.V. Moller, Interaction of membrane proteins and lipids with solubilizing detergents, *Biochim. Biophys. Acta* 1508 (2000) 86–111. <<http://www.ncbi.nlm.nih.gov/pubmed/11090820>>.